Monte Carlo simulation of size, random field and temperature dependences of exchange bias in a core/shell magnetic nanoparticle

2007 J. Phys.: Condens. Matter 19 186202

(http://iopscience.iop.org/0953-8984/19/18/186202)

IOP PUBLISHING JOURNAL OF PHYSICS: CONDENSED MATTER

J. Phys.: Condens. Matter **19** (2007) 186202 (13pp) doi:10.1088/0953-8984/19/18/186202

Monte Carlo simulation of size, random field and temperature dependences of exchange bias in a core/shell magnetic nanoparticle

M H Wu, Q C Li and J-M Liu[1]

Laboratory of Solid State Microstructures, Nanjing University, Nanjing 210093, People's Republic of China
and
International Center for Materials Physics, Chinese Academy of Sciences, Shenyang, People's Republic of China

E-mail: liujm@nju.edu.cn

Received 1 December 2006, in final form 15 February 2007
Published 4 April 2007
Online at stacks.iop.org/JPhysCM/19/186202

Abstract

By using Monte Carlo simulation on a ferromagnetic core/antiferromagnetic shell nanoparticle, we investigate in detail the exchange bias of the magnetic hysteresis as a function of both core radius and shell thickness, at low temperature. It is found that the exchange bias is very sensitive to the core radius and a small variation of the radius may lead to a big fluctuation of the bias. In a general tendency the exchange bias is enhanced by increasing shell thickness and decreasing core radius. The intrinsic correlation between the exchange bias and the spin configuration on the core–shell interface is demonstrated. We further investigate the dependence of the exchange bias on temperature and random field inside the nanoparticle, indicating a monotonic decreasing of the bias with the magnitude of random field and temperature, respectively.

(Some figures in this article are in colour only in the electronic version)

1. Introduction

When a ferromagnetic (FM) component is coherently contacted with an antiferromagnetic (AFM) one and submitted to a continuously decreasing temperature T under an external magnetic field F through the Néel point T_N of the AFM component, where T_N is usually lower than the Curie point T_C of the FM component, a shift of the hysteresis loop along the F-axis will be observed. This effect is known as exchange bias (EB) and represents an essential feature in FM/AFM composite structure and is of special significance for magnetic recording applications [1]. The EB effect was first discovered decades ago in partially oxidized

[1] Author to whom any correspondence should be addressed.

Co particles [2]. To date there have been hundreds of material combinations reported in the search for optimal performances for practical applications [3].

There has been recent interest in the EB effect in magnetic nanostructures because of its promise for high-density magnetic recording and memory, such as in giant magnetoresistive spin-valves and vertical recording geometry. For a review of this topic readers may refer to [4]. A huge amount of theoretical and experimental work on the EB effect as a function of component dimension [5, 6], temperature [7, 8] or interface roughness [9, 10] in layered FM/AFM structures has been reported. It is worth mentioning that core/shell nanoparticles are of interest as potential magnetic recording media, where usually the core is FM and the shell is AFM. In fact, in the earliest work on Co particles, the AFM CoO shell surrounding the FM Co core constituted a core/shell nanoparticle. In such case, the well-ordered nanoparticle assembly constitutes a high-density recording platform. In a magnetic core–shell structure, a significant EB effect can be predicted because of the coherent interface coupling between the core and shell. Although in nanoparticle systems fewer experimental techniques can be applied for characterization of structure and properties [11, 12], many works on microscopic models, especially Monte Carlo (MC) simulations [13, 14], including those partially addressing the EB phenomenon in nanostructures [15], have been presented. However, in the literature on MC simulations, a direct correlation between EB and the delicate spin configuration on the core/shell interfaces is not very clear, since the interfacial spin configurations can be very complicated, as shown below.

It has been found that uncompensated interfacial spins play a crucial role in EB [16–19], which is believed to depend mainly on the interfacial spin configuration and less on the particle size [20]. Therefore these dependences might be explained by inspecting the interfacial spin configurations. It is interesting to note that the spin configuration on the core/shell interface is associated with the core radius in a fascinating manner. In the present paper, we use a simple MC simulation on a cubic model lattice constituting a core/shell nanoparticle to give a detailed investigation of the correlation of EB with the spin configuration on the core/shell interface by varying the core/shell dimensions, random field and temperature.

2. Model and simulation

2.1. Model

We consider a spherical nanoparticle made of a FM core surrounded by an AFM shell in a simple cubic lattice. The spin interaction is described by the Heisenberg model with just the nearest-neighbour interaction for reasons of simplicity. In the presence of an external field F applied along the easy-axis direction (z-axis), the lattice Hamiltonian can be written as [21]:

$$H/k_{\mathrm{B}} = -\sum_{\langle i,j\rangle} J_{ij} s_i \cdot s_j - \sum_i k_i (s_{iz})^2 - h \sum_i s_{iz}, \tag{1}$$

where $\langle i, j\rangle$ refers to the summation over the nearest-neighbouring spin-pairs, J_{ij} is the spin interaction energy which should be separately defined for the core, shell and core–shell interface, i.e. $J_{ij} = J_{\mathrm{sh}}$ for the shell, $J_{ij} = J_{\mathrm{co}}$ for the core and $J_{ij} = J_{\mathrm{int}}$ for the interface; k_i (k_{sh}, k_{co} and k_{int}) are the magnetocrystalline anisotropy factors, $h = \mu F/k_{\mathrm{B}}$ with k_{B} the Boltzmann constant, s_i is the spin moment at site i with magnitude $1/2$ and arbitrary orientation. Because H and $k_{\mathrm{B}}T$ can be given in the same units, here J, T and h are given in the units of K and d in the units of lattice spacing. The first term in equation (1) accounts for the nearest-neighbour spin exchange energy. Similar to earlier work [21], because T_{N} of the AFM shell is usually lower than T_{C} of the FM core, we set $J_{\mathrm{sh}} = -0.5J_{\mathrm{co}} = -5$ K. For simplicity, the exchange for interfacial spins $J_{\mathrm{int}} = \pm J_{\mathrm{sh}}$ is assumed over the whole

simulation, giving $J_{\rm int} = J_{\rm sh}$ for the AFM exchange and $J_{\rm int} = -J_{\rm sh}$ for the FM exchange on the core/shell interface. It will be found below that the sign of $J_{\rm int}$ has no influence on the EB of the particle, although the spin configuration on the core/shell interface can be somewhat different. The second term in equation (1) takes into account the magnetocrystalline anisotropy energy (hereafter, the z-axis is assigned as the easy-axis) which is fixed to $k_{\rm co} = 1$ K for the core and $k_{\rm sh} = 10$ K for the shell, noting that $k_{\rm sh} \gg k_{\rm co}$. The third term is the Zeeman energy in the presence of nonzero h. For the choice of these parameters, we adopt the values given in earlier work [21] so that a comparison between our work and [21] can be made.

2.2. Simulation procedure

We simulate the static magnetic hysteresis loop and equilibrium spin configuration of the core/shell nanoparticle under the adiabatic approximation at very low temperature, followed by a brief discussion on the effect of temperature T in the last section. The simulation is performed based on the Metropolis algorithm. The trial step of the spin updating is a combination of three kinds of trial steps as described by Hinzke and Nowak [22]. Two simulation paths will be employed here. First, the system is cooled from a temperature lower than $T_{\rm C}$ of the core and higher than $T_{\rm N}$ of the shell, equivalent to a step down to $T = 0.1$ K in the presence of $h = h_{FC} = 4$ K along the z-axis. Then at $T = 0.1$ K we cycle the magnetic field between $h = 4$ and -4 K and then back to $h = 4$ K in a step of $\delta h = -0.1$ K by using 300 Monte Carlo steps per spin at each field to evaluate the static hysteresis. Due to the expected EB, we define the half of the hysteresis from $h = 4$ and -4 K as the descending branch (branch I) and the other half (from $h = -4$ to 4 K) as the ascending branch (branch II), noting that the spin configurations on the two branches do not show symmetry around the zero point.

Second, the system is cooled down to $T = 0.1$ K in the same way as above, and then is allowed to reach the equilibrium state under zero-field condition. In this case we account for the spin configuration on the core/shell interface, by which it is possible to evaluate the net magnetization of the shell spins on the core/shell interface (CSIS spins) at zero field.

2.3. Evaluation of exchange bias

The first roadmap is a calculation from the simulated hysteresis. The EB $h_{\rm eb}$ is defined as:

$$h_{\rm eb1} = (h_{\rm c}^{+} + h_{\rm c}^{-})/2, \tag{2}$$

where $h_{\rm c}^{+}$ is the coercivity on the $+h$-axis and $h_{\rm c}^{-}$ is the coercivity on the $-h$-axis of the hysteresis.

Alternatively, $h_{\rm eb}$ can be calculated by correlation with the spin configuration in the core/shell interface, referring to [21]:

$$h_{\rm eb2} = -J_{\rm int}(M_{\rm int}^{+} + M_{\rm int}^{-})/2, \tag{3}$$

where $M_{\rm int}^{\pm}$ is the net magnetization of the CSIS spins at the positive (negative) coercivities, $h_{\rm c}^{\pm}$ respectively, which can be evaluated from the simulated spin configurations at $h_{\rm c}^{\pm}$. In detail, we count all of the CSIS spins at $h = h_{\rm c}^{\pm}$ and sum them along the z-axis to obtain $M_{\rm int}^{\pm}$.

Thirdly, we can also define another EB value by evaluating the net magnetization of the CSIS spins, $M_{\rm int}$, from the equilibrium spin configuration of the nanoparticle under zero field:

$$h_{\rm eb3} = -J_{\rm int} \cdot M_{\rm int}. \tag{4}$$

In the following sections we shall present in detail our investigation of the dependence of $h_{\rm eb}$ on a series of system parameters and core/shell dimensions. In a general sense, the evaluated $h_{\rm eb1}$, $h_{\rm eb2}$ and $h_{\rm eb3}$ are quite consistent with each other.

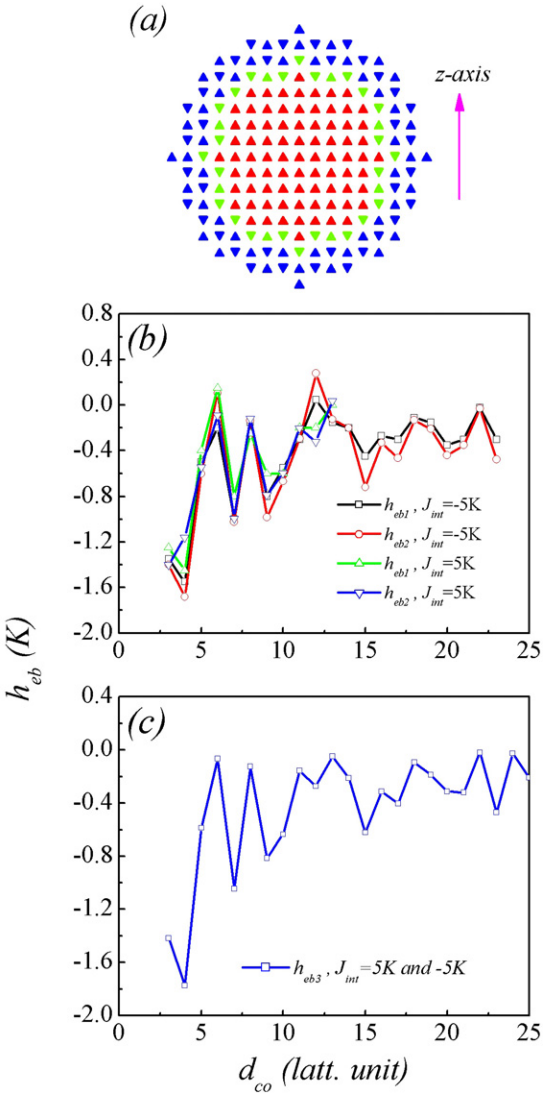

Figure 1. (a) Snapshot of the spin configuration of a cross sectioned core/shell nanoparticle simulated under $h = 4$ K, $J_{\rm int} = -5$ K, $d_{\rm co} = 5$ and $d_{\rm sh} = 3$. Here the red, green and blue (medium, light and dark grey) arrows represent the core spins, the shell spin on the core/shell interface and the shell spins, respectively. (b) Exchange bias $h_{\rm eb}$ as a function of core radius $d_{\rm co}$. The square dots and circular dots represent the data from $M_{\rm int}$ of the CSIS spins (equation (3)) and from the simulated hysteresis (equation (2)) as $J_{\rm int} = J_{\rm sh}$, respectively; and the up-triangle dots and down-triangle dots are for the data from $M_{\rm int}$ of the CSIS spins (equation (3)) and from the simulated hysteresis (equation (2)) as $J_{\rm int} = -J_{\rm sh}$, respectively. (c) $h_{\rm eb}$ as a function of $d_{\rm co}$ as evaluated from equation (3) by counting $M_{\rm int}$ of the CSIS spins at zero field. $d_{\rm sh} = 3$.

3. Results and discussion

3.1. Core radius dependence

We show a typical snapshot of the spin configurations in figure 1(a). Figure 1(b) presents the evaluated $h_{\rm eb1}$ and $h_{\rm eb2}$ as a function of core radius $d_{\rm co}$, respectively, for both $J_{\rm int} = J_{\rm sh}$ (squares

and circles) and $J_{\rm int} = -J_{\rm sh}$ (up triangles and down triangles), given shell thickness $d_{\rm sh} = 3$. In fact, as $d_{\rm sh} > 3$, the results are the same as shown here. In figure 1(c) we plot $h_{\rm eb3}$ as a function of $d_{\rm co}$ as $J_{\rm int} = -5$ K and the results for $J_{\rm int} = 5$ K remain the same. Clearly, it is shown that the evaluated $h_{\rm eb1}$, $h_{\rm eb2}$ and $h_{\rm eb3}$ are quite consistent with each other. From the good consistency of $h_{\rm eb1}$ and $h_{\rm eb2}$, one does not find a significant influence of the sign of $J_{\rm int}(= \pm J_{\rm sh})$ on the evaluated $h_{\rm eb}$.

For the $h_{\rm eb}$–$d_{\rm Co}$ relation, it is observed that upon increasing $d_{\rm Co}$, $h_{\rm eb}$ shows remarkable oscillating behaviour at small $d_{\rm co}$, and then tends to a stable value when $d_{\rm co}$ becomes very large. Although the magnitude of $h_{\rm eb}$ gradually decreases with increasing $d_{\rm co}$ in a general tendency, it is very sensitive to $d_{\rm co}$ for small $d_{\rm co}$. For instance, $h_{\rm eb} \sim -1.7$ K at $d_{\rm co} = 4$, while it becomes $\sim$−0.55 K at $d_{\rm co} = 5$. This high sensitivity and the oscillating behaviour of the $h_{\rm eb}$–$d_{\rm co}$ relation are not favoured from the point of view of practical applications. What should be addressed here is the exceptional case of $d_{\rm sh} = 1$, where some CSIS spins remain partially unpaired and the others are fully bonded with six nearest neighbour (NN) spins. In this case, and $d_{\rm sh} = 2$, the shell spins can no longer hold AFM order and the EB will disappear, which will not be considered in this work.

3.2. Interfacial spin configurations at $J_{int} = -5$ K

The above effects are well-known phenomena and the underlying physics can be understood by analysing the interfacial spin configurations. In fact, the EB is essentially attributed to the net magnetization of all CSIS spins and is unrelated to other shell spins themselves unless the thermally assisted spin reversal takes effect. To highlight our understanding of the EB and also the oscillating behaviours of $h_{\rm eb}$ as a function of $d_{\rm co}$, it will be helpful to analyse the configuration of the CSIS spins and their reversal sequence upon external field cycling. Here we focus on the case of $J_{\rm int} = -5$ K, and a similar analysis can be done for $J_{\rm int} = 5$ K.

As $d_{\rm sh} > 2$, all of the CSIS spins are bonded with six NN spins, of which the possible number of core spins is 1, 2 or 3. Because of the strong anisotropy for the shell spins ($k_{\rm sh} = 10$ K), all shell spins prefer to align along the $\pm z$-axis with small orientation fluctuations. The configuration of the CSIS spins will be determined by the minimization of the Hamiltonian H. One can evaluate the minimum of H by counting the effective field applied to the spins under consideration, where the effective field is the sum of the external field h and the equivalent field imposed by the NN spins.

Take the case of $|h| \leqslant 4$ K($h_{\rm max} = \pm 4$ K) and $|J_{\rm int}| = 5$ K as an example. It is seen that only those CSIS spins with three NN core spins have possibility to flip. For those CSIS spins with two NN core spins (i.e. four NN shell spins), the equivalent field imposed by the four NN shell spins is 4×5 K$/2 = 10$ K, while that imposed by the two NN core spins equals 5 K. Since one has 10 K > 5 K $+ |h|$, those CSIS spins with only two NN core spins are pinned and have no chance to reverse during the field cycle sequence, as long as $|h| < 5$ K and no thermal fluctuations are counted. This analysis also applies to those CSIS spins with only one NN core spin if any. Therefore, the CSIS spins with one or two NN core spins show no response to the external field cycling and thus make no contribution to the hysteresis loop.

Note here that for a core–shell structure, no CSIS spin can have more than three NN core spins. We only need to account for those CSIS spins having three NN core spins. Furthermore, the three NN core spins must be in the same direction, and so do the three NN shell spins. Keeping this feature in mind we can classify all CSIS spins into two categories. If all the NN spins (including NN core spins and NN shell spins) of a CSIS spin are in the same direction, i.e. this spin is in opposite direction to all of its six NN spins, this CSIS spin is defined as a category-B spin (B-spin). Otherwise, the three NN core spins must be in the opposite direction

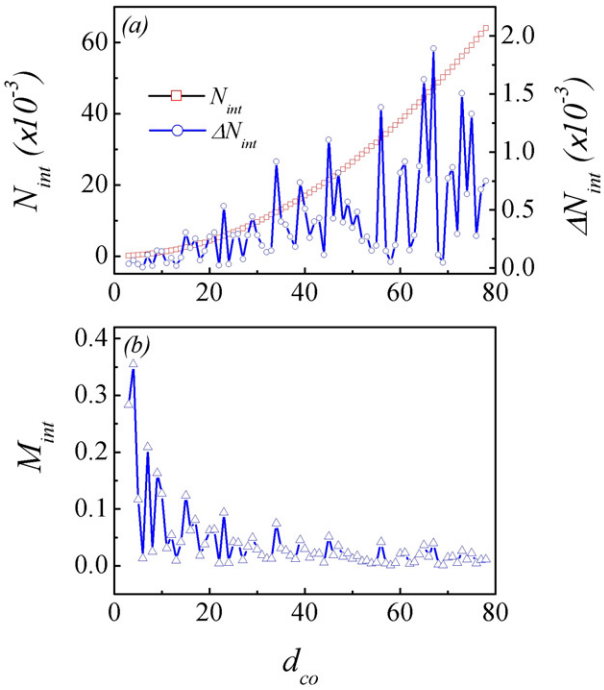

Figure 2. (a) Parameters $\Delta N_{\rm int}$ and $N_{\rm int}$ as a function of $d_{\rm co}$. (b) $M_{\rm int}$ as a function of $d_{\rm co}$. $J_{\rm int} = 5$ K and $d_{\rm sh} = 3$.

to the three NN shell spins, allowing the CSIS spin to be defined as a category-A spin (A-spin). A-spins have the same orientation as their three NN core spins.

We first explain the $h_{\rm eb3}$–$d_{\rm co}$ relation as evaluated from the zero-field equilibrium configuration of the nanoparticle, as shown in figure 1(c). It can be noted that $M^{+}_{\rm int} = M^{-}_{\rm int} = M_{\rm int}$, and $M_{\rm int}$ can be easily calculated. Here we take the case of $d_{\rm co} = 5$ and $d_{\rm sh} > 2$ as an example. Of all 290 CSIS spins, 162 spins align in the same direction and the other 128 spins are in the opposite direction. If $J_{\rm int} = -5$ K, the equivalent field imposed by the NN core spins is always opposite to the external field h during the external field cycling. This equivalent field outweighs the external field, enabling the net magnetization of all the CSIS spins in the opposite direction to the external field and core spins. We obtain $M_{\rm int} = (128 - 162)/290 = -0.11$ and $h_{\rm eb} = -0.55$. Similarly, if $J_{\rm int} = 5$ K, we have $M_{\rm int} = (162 - 128)/290 = 0.11$ and $h_{\rm eb} = -0.55$ too. In this way, we evaluate the EB as a function of $d_{\rm co}$, as shown in figure 1(b).

It is also useful to note that $M_{\rm int} = \Delta N_{\rm int}/N_{\rm int}$, where $\Delta N_{\rm int}$ is the difference between the numbers of CSIS spins with two opposite directions and $N_{\rm int}$ is the total number at zero field. We present $\Delta N_{\rm int}$ and $N_{\rm int}$ as a function of $d_{\rm co}$ in figure 2(a) and then $M_{\rm int}$ as a function of $d_{\rm co}$ in figure 2(b). Clearly, one has $N_{\rm int} \sim d^2_{\rm co}$ while $\Delta N_{\rm int}$ oscillates with increasing $d_{\rm co}$, resulting in an oscillating decreasing behaviour of $M_{\rm int}$ as a function of $d_{\rm co}$, and thus an oscillating behaviour of $h_{\rm eb3}$ against $d_{\rm co}$. However, so far no experimental data on perfect spherical particles are available, and the oscillation behaviour may not be as significant as shown in our simulation. This may explain why only a decreasing EB effect with increasing core radius is observed.

Secondly, we come to explain the $h_{\rm eb2}$–$d_{\rm co}$ relation as shown in figure 1(a). Upon external field cycling, those CSIS spins with three NN core spins may reverse, which may influence the EB. The reversal sequence can be identified from the hysteresis of $M_{\rm int}$ for the CSIS spins

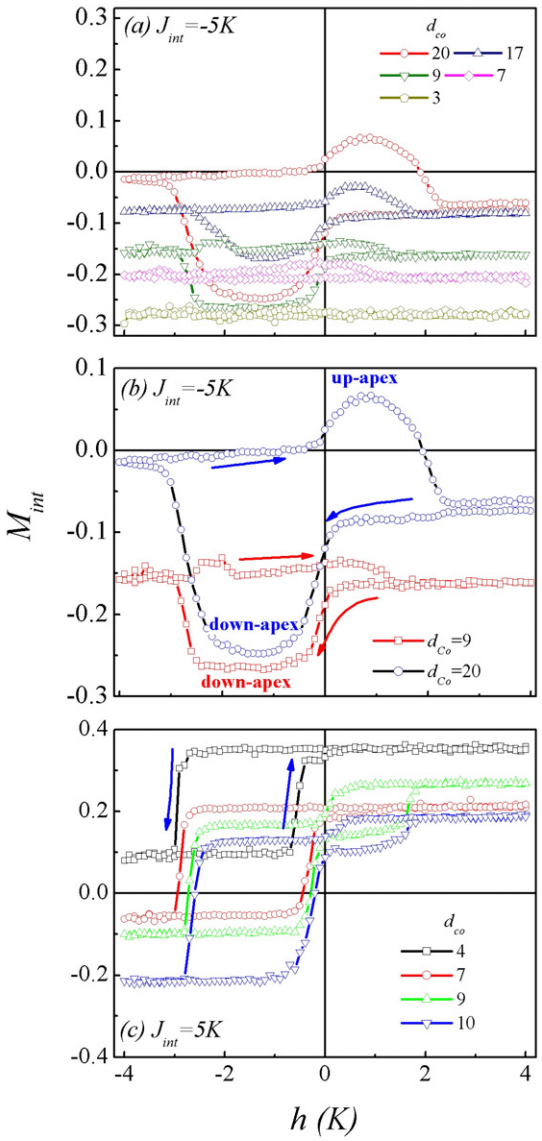

Figure 3. Simulated $M_{\rm int}$–h hysteresis loops at $d_{\rm sh} = 3$ and different $d_{\rm co}$ for (a) $J_{\rm int} = -J_{\rm sh}$, (b) two typical loops of $J_{\rm int} = -J_{\rm sh}$ and (c) $J_{\rm int} = J_{\rm sh}$.

with three NN core spins against external field h. We present the evaluated $M_{\rm int}$–h hysteresis loops at different $d_{\rm co}$ in figure 3(a) for $J_{\rm int} = -5$ K. It is seen that the $M_{\rm int}$–h hysteresis upon different $d_{\rm co}$ is very different, predicting the remarkable fluctuations of the core/shell interface coupling at different $d_{\rm Co}$, which are intrinsically responsible for the oscillating pattern of the $h_{\rm eb}$–$d_{\rm co}$ relation.

We observe the intrinsic relationship between the bias and the pattern of the $M_{\rm int}$–h hysteresis at $J_{\rm int} = -5$ K. If the up- or down-apex of the $M_{\rm int}$–h hysteresis is noticeable, the exchange bias will be small. For details, one may take the $M_{\rm int}$–h hysteresis at $d_{\rm co} = 9$ as an example. We first consider branch I of the hysteresis. At the beginning when $h > 0$,

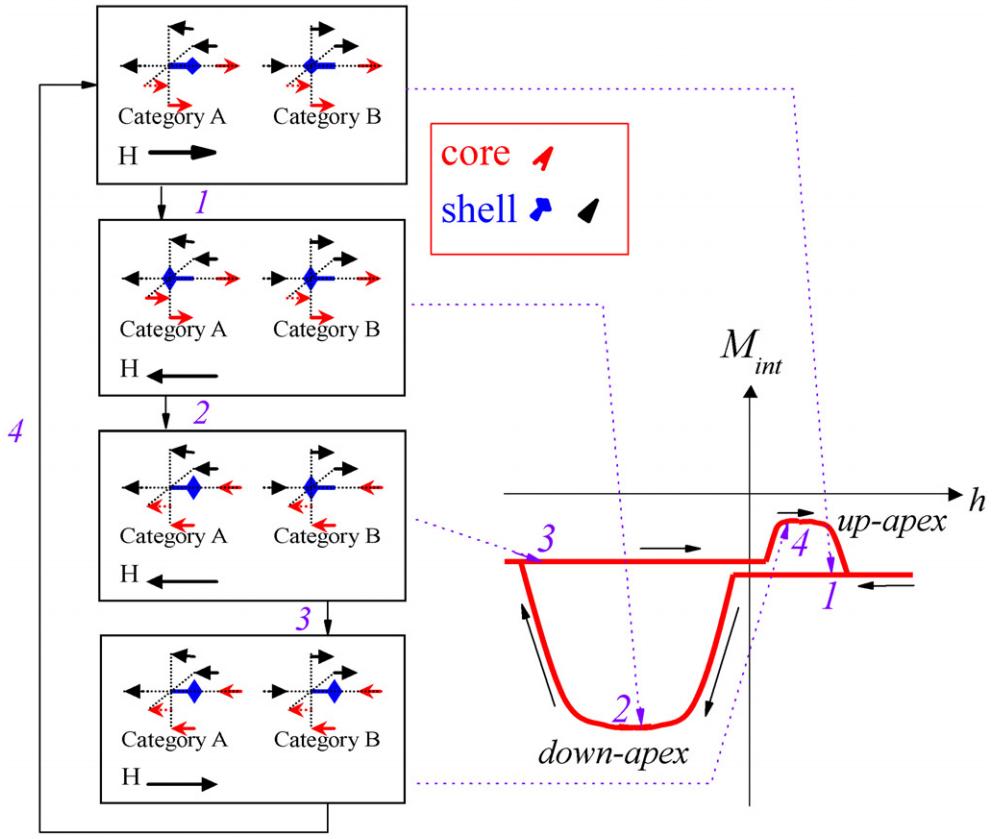

Figure 4. Schematic drawing of the alignments of a CSIS spin (blue) with its six NN spins (red for core spins and black for shell spins) at four different locations (1, 2, 3 and 4) of the M_{int}–h hysteresis. $J_{\text{int}} = -5$ K.

the exchange energy for the A-spins is very small and a small external field h can force them to reverse if they are initially in the opposite direction to h. However, the B-spins are highly stable against an opposite external field h unless h is very large. For the B-spins aligned in parallel to the NN core spins, once h decreases down to a negative value at which the NN core spin reversal occurs, they will turn into A-spins and at the same time those A-spins will turn into B-spins. This sequence can be schematically shown in figure 4 from step 1 to step 2. As $d_{\text{co}} = 9$, there are a total of 918 CSIS spins with 384 spins aligned in the same direction and the other 534 spins are in the opposite direction to the external field h. Therefore, we have $M_{\text{int}} = (384 - 534)/918 = -0.163$, and $h_{\text{eb}} = -J_{\text{int}} \cdot M_{\text{int}} = -0.82$. When h reduces down to zero and becomes negative, 48 A-spins among the total 120 CSIS spins with three NN core spins will reverse, leading to a decrease of M_{int} by $48 \times 2/918 = 0.105$, so $M_{\text{int}} = -0.163 - 0.105 = -0.268$. Furthermore, when h becomes even more negative ($h \sim -3$ K) so that reversal of the core spins occurs, the 48 A-spins will reverse back to their initial state, so M_{int} comes back to -0.163 again. This sequence leads to the appearance of a local down-apex in the M_{int}–h hysteresis, as shown in figure 3(b).

However, for branch II of the hysteresis (step 3 to step 4 in figure 4), the core spins on the core/shell interface should be able to reverse earlier than other core spins [15] because of the negative exchange bias. If the core spins on the interface can reverse before the A-spins, these

A-spins will be unable to reverse, and thus the apex will disappear, as shown in figure 3(b) too. Otherwise, one can observe an up-apex in the hysteresis, like the case of $d_{co} = 20$ as shown in figure 3(b). A similar case applies for $d_{co} = 15$, 17, and 23, as identified in figure 3(a). In case of few A-spins and B-spins, such as for nanoparticles of small core radius $d_{co} = 3$, 5 or 7, we observe no apex in either branch I or II, as shown in figure 3(a).

Sometimes the effect of these apexes on exchange bias is considerable. Take $d_{co} = 9$ stated above for instance, when the apex that appears is taken into account, we obtained $-h_{eb2} = 1.07$, which is larger than $-h_{eb3} = 0.82$ obtained without considering the apex. Besides, both the up-apex and the down-apex contribute to the enlargement of coercivity. According to [21], $h_c = h_c^0 + J_{int}(M_{int}^+ - M_{int}^-)/2$, and both apexes can enlarge $M_{int}^+ - M_{int}^-$. Taking the example of $d_{co} = 9$, its coercivity is increased by $J_{int}(M_{int}^+ - M_{int}^-)/2 = 0.505$ as a result of the apex.

In addition, there is another factor contributing to the difference between h_{eb2} and h_{eb3}. As $d_{co} = 6$ or 12, because of certain configurations, M_{int} is so small that Zeeman energy acting on the surface spins of the AFM component can overcome the AFM–FM exchange interaction. According to [23], the EB will become positive then.

3.3. Interfacial spin configurations at $J_{int} = 5$ K

Although the hysteresis for the whole lattice at $J_{int} = 5$ K remains quite similar to that at $J_{int} = -5$ K, given the same values for other parameters, the mechanism for the EB is different, which can be understood by analysing the M_{int}–h hysteresis. At the beginning of branch I, the number of B-spins, M_{int}, and magnetization of the core M_{co}, are all in the same direction as h. Similarly, when h decreases from the positive maximum $h_{max} = 4$ K (branch I), all B-spins align with the external field, which will reverse as h reduces down to zero and becomes negative. This will lead to a decreasing step in M_{int}, as shown in figure 3(c) at $d_{co} = 9$ and 10. Meanwhile, all the A-spins remain in the same direction as the core spins. As long as h further decreases down to a negative value at which the NN core spins begin to reverse, the earlier B-spins will turn into A-spins and vice versa. Consequently, a tremendous drop M_{int} will be expected, accompanied by transfer of the earlier A-spins into B-spins. A similar sequence will occur when h increases from the negative maximum $-h_{max} = -4$ K (branch II), which leads to two increasing steps in branch II of the $M_{int} - h$ hysteresis.

However, it is observed in figure 3(c) that as $d_{co} = 4$ and 7, we observe only one decreasing step on branch I and one increasing step on branch II. The reason for this is that for the two cases the number of B-spins is very limited so that the other step is too small to be identified. In general, for any d_{co}, if the number of B-spins is comparable to that of A-spins, one will observe two steps on each branch of the hysteresis, otherwise only one step on each branch can be observed.

3.4. Shell thickness dependence

In this section, we come back to study h_{eb} as a function of d_{sh}. It is easily understood that the dependence of h_{eb} on d_{sh} makes sense only at $d_{sh} = 1$, 2 and 3, beyond which no dependence of h_{eb} on d_{sh} is expected. The simulated results are presented in figure 5(a) and (b) for $J_{int} = -5$ K and 5 K, respectively. At $d_{sh} = 1$, most of the CSIS spins are partially unpaired with only four or five NN spins. Since the AFM spin exchange energy is not large enough to resist the interfacial spin interaction, almost all of the shell spins will reverse in association with the reverse of the core spins in response to cycling of the external field h. Also because of very unstable AFM shell spins, one has $M_{int}^+ \sim -M_{int}^-$, leading to $h_{eb} \sim 0$, as shown in both figures 5(a) and (b) for $d_{sh} = 1$.

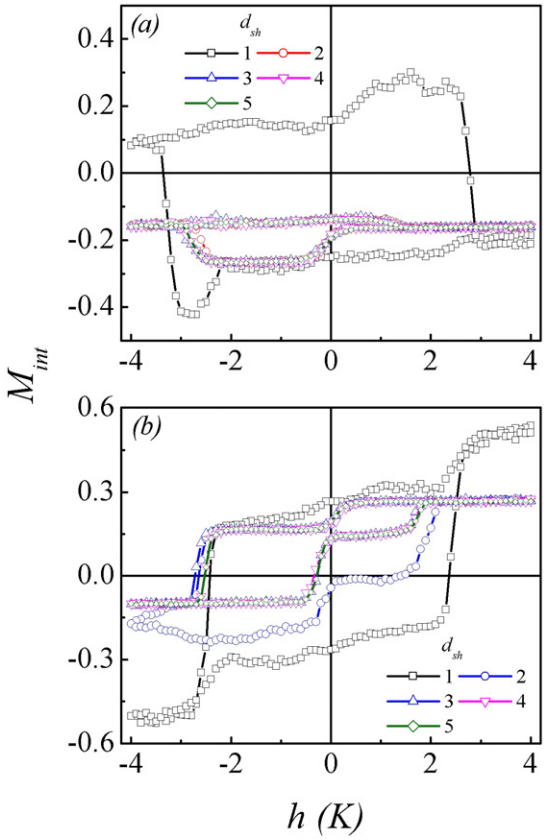

Figure 5. Simulated M_{int}–h hysteresis loops at $d_{\text{co}} = 9$ and different d_{sh} for both (a) $J_{\text{int}} = -J_{\text{sh}}$ and (b) $J_{\text{int}} = J_{\text{sh}}$.

Once $d_{\text{sh}} = 2$ and more, all the CSIS spins have six NN spins. If $J_{\text{int}} = -5$ K, referring to figure 5(a), the hysteresis remains unchanged with increasing d_{sh} once $d_{\text{sh}} > 1$. For $J_{\text{int}} = 5$ K, h_{eb} no longer changes as $d_{\text{sh}} > 2$, as shown in figure 5(b). This indicates that the shell spins (excluding those CSIS spins) are offered sufficiently high stability against reversal of the core spins so long as $d_{\text{sh}} \geqslant 2$. In such cases, the results presented in sections 3.2 and 3.3 make sense.

3.5. Effect of random field

In real materials, the spin interaction cannot be spatially homogeneous and always includes an internal random field to some extent. We also investigate the effect of random field on the exchange bias. In this work, the random field applied to the lattice is assumed to follow the Gaussian distribution:

$$f(J) = \frac{1}{\sqrt{2\pi}\, j} \mathrm{e}^{-\frac{(J-J_0)^2}{2j^2}}, \tag{5}$$

where j is the variance of exchange interaction J, which should be separately defined for the core, shell and core–shell interface, i.e. $j = j_{\text{sh}}$ for the shell, $j = j_{\text{co}}$ for the core and $j = j_{\text{int}}$ for the core/shell interface. The value of J, J_0, is set at $J_0^{\text{shell}} = -5$ K for the shell, $J_0^{\text{core}} = 10$ K for the core and $J_0^{\text{int}} = -5$ K for the core/shell interface. We

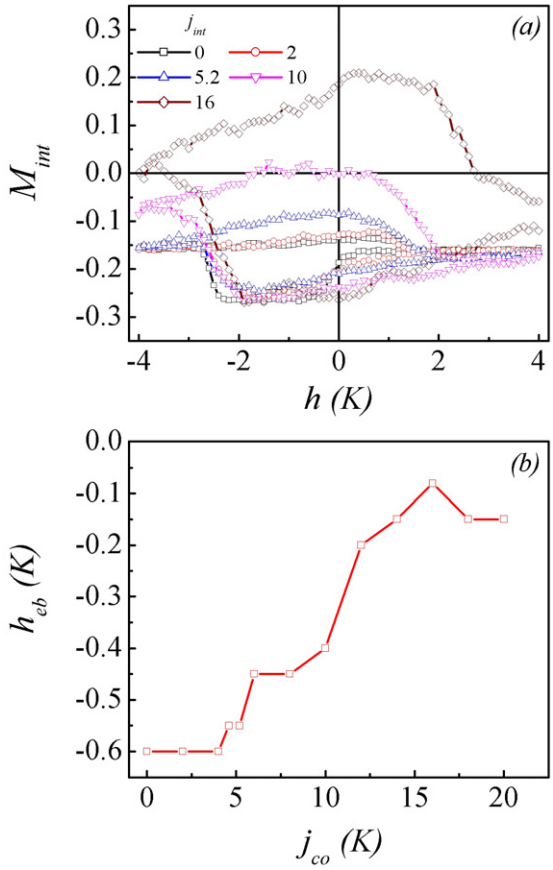

Figure 6. (a) Simulated $M_{\rm int}$–h hysteresis loops under different $j_{\rm co}$. (b) Exchange bias $h_{\rm eb}$ as a function of $j_{\rm co}$. $J_{\rm int} = -5$ K, $d_{\rm co} = 9$ and $d_{\rm sh} = 3$.

set $j_{\rm co}$:$j_{\rm int}$:$j_{\rm sh} = |J_0^{\rm core}|:|J_0^{\rm int}|:|J_0^{\rm shell}| = 2{:}1{:}1$, $d_{\rm co} = 9$ and $d_{\rm sh} = 3$ in our simulation as a demonstration. Because the variance of the sum of independent random variables equals the sum of each variable's variances, for a CSIS spin with three NN core spins, the variance of the equivalent field imposed by the six NN spins is $j_{\rm NN} = \sqrt{3 \times 1^2 + 3 \times 0.5^2}\, j_{\rm Co} \approx 1.94\, j_{\rm co}$. For a CSIS spin with two NN core spins, $j_{\rm NN} = \sqrt{2 \times 1^2 + 4 \times 0.5^2}\, j_{\rm Co} \approx 1.73\, j_{\rm co}$.

The simulated $M_{\rm int}$–h hysteresis loops under different random field amplitudes $j_{\rm co}$ are shown in figure 6(a). As $j_{\rm co} > 0$, the exchange energy of some A-spins becomes nonzero. When h crosses over zero from a positive value, those A-spins with positive exchange energy will reverse, while those with negative exchange energy may not, depending upon the magnitude of the random field $j_{\rm co}$. As mentioned earlier in section 3.2, for $j_{\rm co} = 0$, no apex on the hysteresis will be possible when h increases from $-h_{\rm max}$ (branch II), since the core spins will reverse before to the A-spins. However, as $j_{\rm co} > 0$, some A-spins with positive exchange energy may reverse before the core spins reverse, resulting in the apex in the hysteresis once more, although the apex is relatively diffuse. This effect is clearly shown in figure 6(a), and it will be more significant when $j_{\rm Co}$ is larger.

As $j_{\rm co}$ reaches up to 4.1 K and more, for branch II more and more A-spins have their exchange energy surpassing $j_{\rm NN}/2 = 1.94\, j_{\rm co}/2 = 4$ K. The equivalent field imposed by their NN spins outweighs the external field, which enables them to reverse to the positive direction

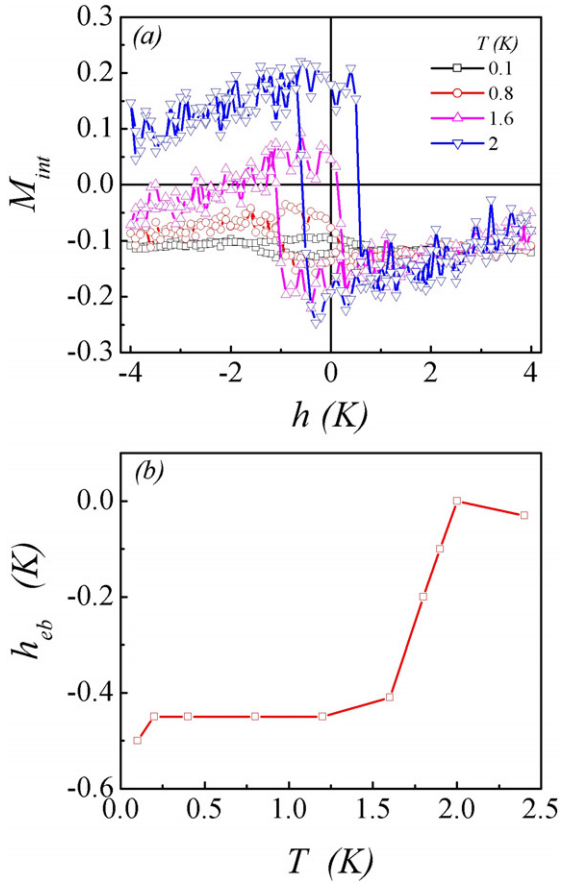

Figure 7. (a) Simulated $M_{\rm int}$–h hysteresis loops under different temperature T. (b) Exchange bias $h_{\rm eb}$ as a function of T (the error of data is ∼5%). $J_{\rm int} = -5$ K, $d_{\rm co} = 5$ and $d_{\rm sh} = 3$.

before h increases to zero and becomes positive. Meanwhile those with negative exchange energy remain unreversed, acting as if there were no random field. As a result, $M_{\rm int}^{+}$ will rise and $|h_{\rm eb}|$ will decrease rapidly.

When $j_{\rm co}$ approaches 10.4 K and goes on increasing, more and more other shell spins (for example, those shell spins with two NN core spins as shown in figure 2) become capable of reversing when the core spins begin to reverse on branch I, because their exchange energy exceeds $(j_{\rm NN} - 10\ {\rm K})/2 = (1.73 j_{\rm co} - 10\ {\rm K})/2 = (18\ {\rm K} - 10\ {\rm K})/2 = 4$ K and outweighs the external field. At the same time, those with negative exchange energy remain stable. Thus $M_{\rm int}$ is greatly enhanced at the beginning of branch II, and $|h_{\rm eb}|$ will continue decreasing as a result of rising $M_{\rm int}$. When j attains some certain value, $|h_{\rm eb}|$ gradually stops declining.

3.6. Temperature dependence

Finally, we simulate the temperature effect on the EB, where temperature T is included in the Metropolis algorithm of the simulation. The simulated $M_{\rm int}$–h hysteresis loops under different T for nanoparticles of $d_{\rm co} = 5$, $d_{\rm sh} = 3$ and $J_{\rm int} = -5$ K are shown in figure 7(a). As T increases, fluctuations of the curve become more and more considerable, while the antiferromagnetism of the shell diminishes. As T approaches $T_{\rm N}$, every shell spin receives

less and less exchange energy from its NN shell spins to stabilize itself due to the declining antiferromagnetism. As a result, more CSIS spins will reverse simultaneously with the reversal of the core spins, which causes the decreasing difference between the absolute values of $M_{\rm int}^{+}$ and $M_{\rm int}^{-}$. At $T \approx T_{\rm N} = 2.0$ K, where the AFM order of the shell disappears, all the CSIS spins receive zero exchange energy from the NN shell spins and are able to reverse once their NN core spins reverse; therefore $M_{\rm int}^{+} = -M_{\rm int}^{-}$, $h_{\rm eb} = 0$, as shown in figure 7(b). This temperature is known as the blocking temperature $T_{\rm B}$, and our explanations above clarify the phenomenon $T_{\rm B} \approx T_{\rm N}$ in high quality thin film systems with thick AFM layers [4].

4. Conclusion

In summary, through MC simulations based on the core/shell nanoparticle model, we have investigated in detail the dependences of the EB on both core radius and shell thickness. It has been demonstrated that the EB is very sensitive to the core radius. A remarkable oscillating behaviour of the bias with increasing core radius for small radii has been identified, although in a rough sense the bias is higher when the core radius is smaller. A large bias is favoured for a thick shell. Investigations of the interfacial spin configuration and its correlation with the EB enable us to understand the underlying physics. By similar methods we have investigated the dependence of the EB on random field and temperature, and we find that EB is reduced monotonically by the enhancement of random field and temperature.

Acknowledgments

The authors thank the Natural Science Foundation of China (10674061, 50332020) and National Key Projects for Basic Research of China (2002CB613303, 2006CB921802).

References

[1] Nogues J and Schuller I K 1999 *J. Magn. Magn. Mater.* **192** 203
[2] Meiklejohn W H and Bean C P 1957 *Phys. Rev.* **105** 904
[3] Dieny B, Speriosu V S, Parkin S S P, Gurney B A, Baumgart P and Wilhoit D R 1991 *J. Appl. Phys.* **69** 4774
[4] Nogues J, Sort J, Langlais V, Skumryev V, Surinach S, Munoz J S and Baro M D 2005 *Phys. Rep.* **422** 65
[5] Jungblut R, Coehoorn R, Johnson M T, de Stegge J and Reinders A 1994 *J. Appl. Phys.* **75** 6659
[6] Tsunoda M, Tsuchiya Y, Konoto M and Takshashi M 1997 *J. Magn. Magn. Mater.* **171** 29
[7] Wee L, Stamps R L and Camley R E 2001 *J. Appl. Phys.* **89** 6913
[8] Nowak U and Usadel K D 2002 *Phys. Rev.* B **66** 014430
[9] Moran T J, Gallego J M and Schuller I K 1995 *J. Appl. Phys.* **78** 1887
[10] Shen J X and Kief M T 1996 *J. Appl. Phys.* **79** 5008
[11] Chen M, Yamamuro S, Farrell D and Majetich S 2003 *J. Appl. Phys.* **93** 7551
[12] Cho S J, Kauzlarich S M, Olamit J, Liu K, Grandjean F, Rebbouh L and Long G J 2004 *J. Appl. Phys.* **95** 6804
[13] Eftaxias E, Trohidou K N and Binns C 2004 *Phys. Status Solidi* c **1** 3361
[14] Suess D, Kirschner M, Schrefl T and Fidler J 2003 *Phys. Rev.* B **67** 054419
[15] Mejia-Lopez J, Soto P and Altbir D 2005 *Phys. Rev.* B **71** 104422
[16] Ohldag H, Regan T J, Stöhr J, Scholl A, Nolting F, Lüning J, Stamm C, Anders S and White R L 2001 *Phys. Rev. Lett.* **87** 247201
[17] Ohldag H, Scholl A, Nolting F, Arenholz E, Maat S, Young A T, Carey M and Stöhr J 2003 *Phys. Rev. Lett.* **91** 017203
[18] Kappenberger P, Martin S, Pellmont Y, Hug H J, Kortright J B, Hellwig O and Fullerton E E 2003 *Phys. Rev. Lett.* **91** 267202
[19] Blomqvis P, Krishnan K M and Ohldag H 2005 *Phys. Rev. Lett.* **94** 107203
[20] Eftaxias E and Trohidou K N 2005 *Phys. Rev.* B **71** 134406
[21] Iglesias O, Batlle X and Labarta A 2005 *Phys. Rev.* B **72** 212401
[22] Hinzke D and Nowak U 1999 *Comput. Phys. Commun.* **121/122** 334
[23] Kirk T L, Hellwig O and Fullerton E E 2002 *Phys. Rev.* B **65** 224426